Low-temperature synthesis, characterization and photocatalytic properties of lanthanum vanadate LaVO4

S. Lotfi, M. El Ouardi, H. Ait Ahsaine, Véronique Madigou, A. Baqais, A. Assani, M. Saadi, Madjib Arab

Heliyon 9 (2023) e17255

Contents lists available at ScienceDirect

Heliyon

journal homepage: www.cell.com/heliyon

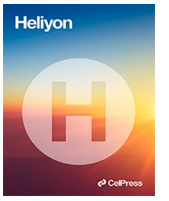

Low-temperature synthesis, characterization and photocatalytic properties of lanthanum vanadate $LaVO_4$

S. Lotfi [a], M. El Ouardi [a,b], H. Ait Ahsaine [a,*], V. Madigou [b], A. BaQais [c], A. Assani [a], M. Saadi [a], M. Arab [b]

[a] Laboratoire de chimie appliquée des matériaux, faculté des sciences, Mohammed V University in Rabat, Morocco
[b] Institut Matériaux Microélectronique et Nanoscience du Provence IM2NP, UMR, CNRS, Université du Sud Toulon-Var, France
[c] Department of Chemistry, College of Science, Princess Nourah Bint Abdulrahman University, Riyadh, Saudi Arabia

ARTICLE INFO

Keywords:
Lanthanum vanadate
Photocatalysis
Dye degradation
Optical properties

ABSTRACT

In this study, we have successfully prepared tetragonal lanthanum vanadate $LaVO_4$ nanoparticles by a facile co-precipitation method at room temperature. The obtained materials were characterized using different structural and micro-structural techniques such as the characterization by X-ray diffraction (XRD), UV–Vis diffuse reflectance spectrum (DRS), transmission electron microscopy (TEM), and Raman spectrometry. The obtained structure is crystallized in single tetragonal phase with pin-like nanostructure. A main optical transition with bandgap energy of 3.26 eV is evidenced, and the average lifetime of charges carriers was found to be 1 ns Furthermore, the photoluminescence occurs in the visible light range. The photocatalytic activity was evaluated by the photocatalytic degradation of methylene blue (MB) with initial concentration of 10 mg L^{-1}. The result indicates that $LaVO_4$ particles showed a best photocatalytic activity of 98.2% degradation for methylene blue solution after irradiation of 90 min under visible light. Furthermore, the photocatalytic mechanism and reusability were studied.

1. Introduction

Recently, water pollution has been a major issue for many societies across the World. However, The discharge of contaminants from various manufacturing sectors such as plastics, cosmetics, textile, as well as pharmaceutical and food industries [1,2] posed a serious threat to water resources [3,4]. 800,000 tons of dyes are generated each year, and 140,000 tons are discharged in wastewater leading to adverse impacts on both human health as well as on the environment [5]. In this context it is reported that about 3.2 million persons die annually because of these poisonous contaminants [6]. Therefore, a number of physical, biological, and chemical water treatment procedures [7] have been employed such membrane filtration [8,9], adsorption [10,11], coagulation-flocculation [12,13], biological treatments [14] and ion exchange [15], in order to remove the organic dyes from water [16]. Unfortunately these conventional treatment processes are not effective for the mineralization of non-biodegradable substances and involve significant energy consumption and cost [17,18]. On the other hand, advanced oxidation technologies, especially photocatalytic degradation based on heterogeneous catalysis, have attracted significant interest because of its high efficiency regarding organic dyes, its easy and cost-effective setup. They are promising technologies for partial or complete mineralization of dyes into CO_2 and water [19–23]. Thus, photocatalysis is an efficient and sustainable technology to remove synthetic dyes from wastewater [16,24], operating under sunlight

* Corresponding author.
E-mail address: h.aitahsaine@um5r.ac.ma (H. Ait Ahsaine).

https://doi.org/10.1016/j.heliyon.2023.e17255
Received 2 March 2023; Received in revised form 12 June 2023; Accepted 12 June 2023
Available online 13 June 2023

irradiation in order to create strong redox systems which are able to degrade the molecules in both aquatic and gaseous environments [25,26]. As is known, many researchers have developed photo-catalysts based on tungstates [27–32], vanadates [33,34], molybdates [35], metal–organic frameworks [36,37] for the degradation of the organic pollutants and the depollution of wastewater [32]. Recently, ortho-vanadates ($InVO_4$, $BiVO_4$, $CeVO_4$, $SmVO_4$, $FeVO_4$ etc.) have received special consideration in photocatalytic degradation technology on account of the characteristics provided by the vanadium metal which exhibits electrons on the 3d orbital. These electrons can be activated by visible light and then participate in the decomposition reaction of organic contaminants [17,38–41]. Among them, lanthanide orthovanadates $LaVO_4$ was considered as one of promising photocatalytic materials due to its catalytic performance, great optical properties owing to its unique electronic structure, and the absorption of visible light [42–44]. It primarily exists in two crystalline polymorphs, namely tetragonal phase (t) with zircon structure and monoclinic phase (m) with monazite structure [45–47]. $LaVO_4$ chooses the monazite type as a strong tendency because it is characterized by its higher oxygen coordination number of 9, in contrast zircon type with a number of 8 [45,48]. Thus, It is thermodynamically stable but it does not possess superior properties as compared to zircon [45,49]. The results show that t-$LaVO_4$ has an excellent thermal stability, a direct band gap, a small size of particles and high optical absorption. In contrast, m-$LaVO_4$ has an indirect band gap. As a result, it was confirmed that the promising properties of this structure have a positive influence on the catalytic properties.

Generally, $LaVO_4$ was prepared by sol-gel [44,50], hydrothermal [45], citrate method [51] and microwave methods [52] that used organic additives or surfactants and thermal treatment process [53–56], which will increase the production costs and also produce new organic pollutants. The researchers developed a different number of catalysts by green synthesis such as ($MgFe_2O_4$@$CoCr_2O_4$ [7], CuO [2], $MgFeCrO_4$ [16], $Mg_{0.5}Fe_{0.5}MnO_4$ [24], $Ni_{0.25}Fe_{0.75}Fe_2O_4$ [57], $NiFe_2O_4$@ZnO [58] and $CoMnCrO_4$ [59]).

Herein, we report the preparation of non-calcined t-$LaVO_4$ at room temperature via co-precipitation process. The synthesis of $LaVO_4$ photocatalyst at ambient temperature is a novel synthesis strategy with a potential to address some of the challenges associated to traditional high-temperature synthesis methods. The as-synthesized catalyst was characterized by XRD, DRS, TEM, and Raman spectrometry. The photocatalytic activity of $LaVO_4$ was evaluated as a photocatalyst for Methylene Blue degradation in aqueous solution under light irradiation.

2. Experimental section

2.1. Materials and reagents

The reagents employed to synthesize these semiconductor photocatalysts comprise: lanthanum nitrate hexahydrate ($La(NO_3)_3.6H_2O$, 99.9%, Fisher Scientific), ammonium metavanadate (NH_4VO_3, 99.5%, ACROS Organics), nitric acid (HNO_3 65%, Merck) and sodium hydroxide (NaOH, 99%, Fisher Scientific).

2.2. Synthesis of $LaVO_4$

The nanocrystalline $LaVO_4$ was prepared by a co-precipitation method. In a typical process, a quantity of NaOH and NH_4VO_3 were firstly dissolved in 20 mL distilled water to form a Na_3VO_4 aqueous solution. Then, $La(NO_3)_3{\cdot}6H_2O$ nitrate was dissolved in 15 mL of distilled water and 5 mL of 1 M nitric acid, this aqueous solution was added drop-wise to the first mixture under constant magnetic stirring. After 2 h of stirring, the pH value of the mixture was adjusted to about 7 by using sodium hydroxide solution. The mixture was maintained under continuous stirring for 30 min. The resultant solution was filtered as well as washed with distilled water and the precipitate was dried at 80 °C for 3 h and finely ground.

2.3. Material characterizations

The samples were characterized by X-ray diffraction (XRD; EMPYREAN Panalytical diffractometer) with Cu Kα radiation (λ = 1.5406 Å) ranging from 10 to 70° with a step size of 0.028° and a scanning speed of 0.001° $2\Theta.s^{-1}$. Raman spectra were recorded at room temperature by using a RENISHAW spectrometer equipped with a 633 nm laser (30 s exposure time). Morphologies of the prepared samples were examined by transmission electronic microscopy (TEM: Tecnai G^2 200 kV with a LaB_6 source). Electron dispersion spectroscopy (EDS) connected to the SEM was employed to observe the chemical composition of the samples. UV–vis diffuse reflectance spectra (DRS) obtained in the wavelength region of 200–800 nm, using UV–Vis spectro-photometer (JASCO UV–Vis V-730). The luminescence and the time-resolved fluorescence emission decay measurements were collected through fluorescence spectrophotometer (FLUOROMAX, HORIBA).

2.4. Photocatalytic procedure

The photocatalytic activity of as-fabricated $LaVO_4$ sample was evaluated by the degradation of methylene blue (MB) under light irradiation using Philips lamps 300 W. Firstly, 100 mg of $LaVO_4$ was dissolved in 100 mL of MB solution (3.1×10^{-5} M) in pH of 4.85. Then, the solution was sonicated for 15 min and agitated in dark for 1 h to get absorption/desorption equilibrium of MB with $LaVO_4$. Then, the reaction mixture was illuminated by visible light Philips lamps (300 W) under constant stirring using a magnetic stirrer. 3 mL of the suspension was harvested and centrifuged for 12 min at 13 200 rpm to separate the $LaVO_4$ powder from the solution. The decomposition evolution of MB was followed with the Shimadzu UV 2600 spectrophotometer registering the absorbance in the wavelength range 200–800 nm. In this (L-ascorbic acid; $O2^{-}$), isopropanol (IPA; $OH^{\cdot}$), disodium ethylenediaminetetraacetate (EDTA;

h^+) were used as reaction scavengers to indicate the contribution of active species into the photocatalytic pathway.

2.5. Zero charge point measurement

The point of zero charge pH_{pzc} corresponds to the pH value at which the surface charge is equivalent to zero. 50 mg of the sample was placed in six flasks that contained 50 mL of a 0.1 M potassium nitrate solution. The initial pH value of these solutions has been tuned to 2, 4.07, 6.27, 8.27, 10.13 and 12.09 using a few drops of 0.1 M nitric acid (HNO_3) or 0.1 M sodium hydroxide (NaOH). The resulting solution was stirred for 24 h. The resulting suspension was filtered, and then the final pH value was measured.

2.6. Chemical oxygen demand (COD)

MB photo-decomposition tests have been carried in a 100 mL beaker at ambient temperature. The bath experiment involves the solution to be treated, at a concentration of 10 mg/L, with amount of photo-catalyst. The chemical oxygen demand (COD) was read using a Lovibond COD kit and the resulting data was interpreted using an MD 200 COD spectrophotometer. The photo degradation rate was given as COD_t/COD_0 versus time. This rate was calculated for several reaction times by the formula in equation (1) below:

$$COD(\%) = \left(\frac{COD_0 - COD_t}{COD_0}\right) * 100 \quad (1)$$

COD_0: COD concentration (mg/L of O_2) before degradation and COD_t: COD concentration (mg/L of O_2) at a value of time t.

3. Results and discussion

3.1. Structural analysis

Fig. 1 presents the XRD pattern of the obtained sample, all the peaks could be indexed according to the tetragonal phase of $LaVO_4$ (JCPDS No. 411083). It displays peaks at 18.01°, 23.93°, 30.19°, 32.23°, 34.06°, 38.82°, 43.18°, and 47.59° that correspond to the (101), (200), (211), (112), (220), (301), (103), (312) crystal planes of tetragonal $LaVO_4$, respectively. These results are in good consistency with those of Jie et al. [60].

We calculated the size of the crystallites using the Scherrer method, which can be expressed as in equation (2) [22,61]:

$$D = k\lambda/\beta\cos(\theta) \quad (2)$$

In this equation, D represents the size of the crystallite, λ is the wavelength of radiation and θ is the Bragg angles in radians. The integral breadth β value was calculated using a Gaussian approximation of peak profiles such as $\beta^2 = \Delta(2\theta)^2_{samp} - \Delta(2\theta)^2_{stand}$. $\Delta(2\theta)^2_{samp}$ and $\Delta(2\theta)^2_{stand}$ are respectively the full width at half maximum (FWHM) of Bragg peak of the synthesized samples and the standard sample.

The constant k has a value of 0.9 and assumes that the profiles are gaussian-like. The calculated crystallite size was 18 nm.

3.2. Vibrational analysis

Raman spectra reported that peaks at about 200 cm^{-1} and 1000 cm^{-1} Fig. 2, as a result, seven Raman modes have been detected, they could be attributed to t-$LaVO_4$ phase according to reported data [62,63]. The peaks observed at low values (under ~500 cm^{-1})

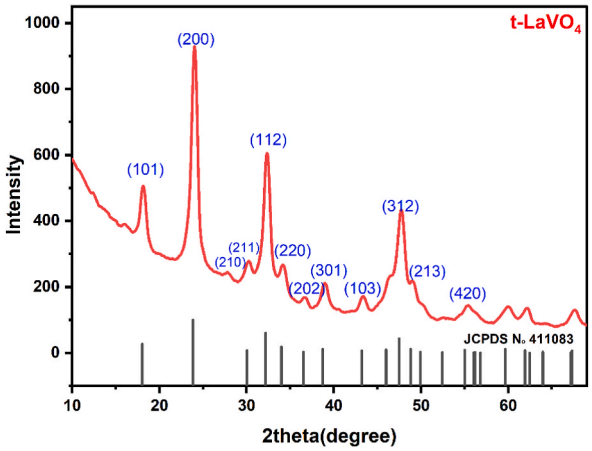

Fig. 1. XRD pattern of t-$LaVO_4$ synthesized by co-precipitation.

can be assigned to La–O vibrations, the high signal at ~ 866 cm^{-1} corresponds to the stretching mode of the V–O (ν1(Ag)) bond. On the other hand, the theoretical group computations 33 optical modes which contain 12 Raman active modes: 5 Eg + $4B_{1g}$ + $2A_{1g}$ + B_{2g}. These modes may be divided in internal (ν_1, ν_2, ν_3 and ν_3) and external (translational T & rotational R) modes of the VO_4 units as following [63]:

$U = A_{1g}(v_1, v_2) + B_{1g}(2T, v_3, v_4) + B_{2g}(v_2) + E_g(2T, R, v_3, v_4)$. We conclude that the observed Raman bands correspond to those of the t-$LaVO_4$ phase which confirms the results of XRD analysis.

3.3. Morphological analysis

The morphology of t-$LaVO_4$ has been investigated by TEM observations (Fig. 3a). It is difficult to determine exactly the form of the particles: some of them are elongated (large:10 nm, length: 25–30 nm) and the other are shapeless. Moreover, they are piled on top of each other as can be seen in Fig. 3a. The size of individual particles was not measured. The electronic diffraction pattern Fig. 3b corresponds to a diffraction of several particles, it shows a series of punctuated rings, this look is characteristic of small crystallized grains. All the diffracted spots correspond to the planes of the tetragonal phase of $LaVO_4$ (they are labelled on Fig. 3b). These results are in good agreement with those of the X-Ray diffraction. We can deduce the crystalline character of the synthesized t-$LaVO_4$. The chemical composition of the material was control by EDS analysis (Fig. 3c). The semi quantitative analysis results are: 59 ± 1 at.% of La and 41 ± 1 at.% of V which leads to an excess lanthanum composition. This difference with the nominal composition may be due to an overlap of the lanthanum and vanadium peaks in the EDS spectra and therefore to an erroneous deconvolution. To refine the composition, it will be necessary to make an analysis with a device better resolved in energy.

3.4. Optical characteristics

Fig. 4a illustrate the diffuse reflectance spectrum of LVO with an outstanding optical absorption in range from 267 nm to 552 nm. This excellent absorption was due to the charge transfer transitions (CT) involve electronic transition from O to V ligands inside the VO_4^{3-} groups [64]. Generally, in vanadate semiconductors, the conduction band is mostly completed by V-3d electrons, whereas the valence band is mostly completed by O-2p electrons. The band gap energy (Eg) has been calculated by using the Tauc's equation $(\alpha h\nu)^{1/\gamma} = B(h\nu - Eg)$ [65], in which (h: Planck's constant, α: absorption coefficient, ν: frequency of the photon, and γ: coefficient = 1/2 or 2 for both direct or indirect band gaps). Several studies indicated that tetragonal $LaVO_4$ has a direct gap band gap (γ = 1/2) [66]. The value E_g = 3.26 eV was estimated from the plot of $(\alpha h\nu)^2$ as function of hν (Fig. 4b).

Photoluminescence spectroscopy (PL) is linked to the activity of photo-generated charge carriers. As can be noticed in Fig. 4c, The luminescence spectra show two main emission bands centered at respectively at 467 nm and at 568 nm. According to the UV–Vis spectra, the low emission at 467 nm corresponds to the band-edge electronic transition around the bandgap, while the strong emission at 568 nm is due to the transition from the defects energy levels localized in the bandgap.

. These emissions are related to the charge transfer from oxygen 2p to vanadate 3d orbitals inside the tetrahedral VO_4^{3-} groups [67]. They might also come from defects generated by other V ions [68]. The decay curve for $LaVO_4$ is presented in Fig. 4d. We should note that the excitation wavelength was set at 284 nm while the emission wavelength was set at 468 nm. The fitting of the decay plot using two models of mono-exponential and bi-exponential decay equations showed that the decay analysis follows a bi-exponential decay. The bi-exponential fit was performed according to equation (3) that is given as follows:

$$I_t = I_1\, e^{-(t/\tau 1)} + I_2\, e^{-(t/\tau 2)} \quad (3)$$

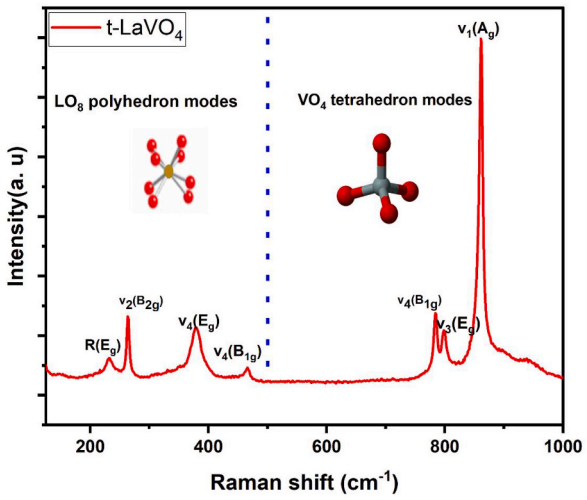

Fig. 2. Raman spectrum of t-$LaVO_4$ NPs obtained at room temperature.

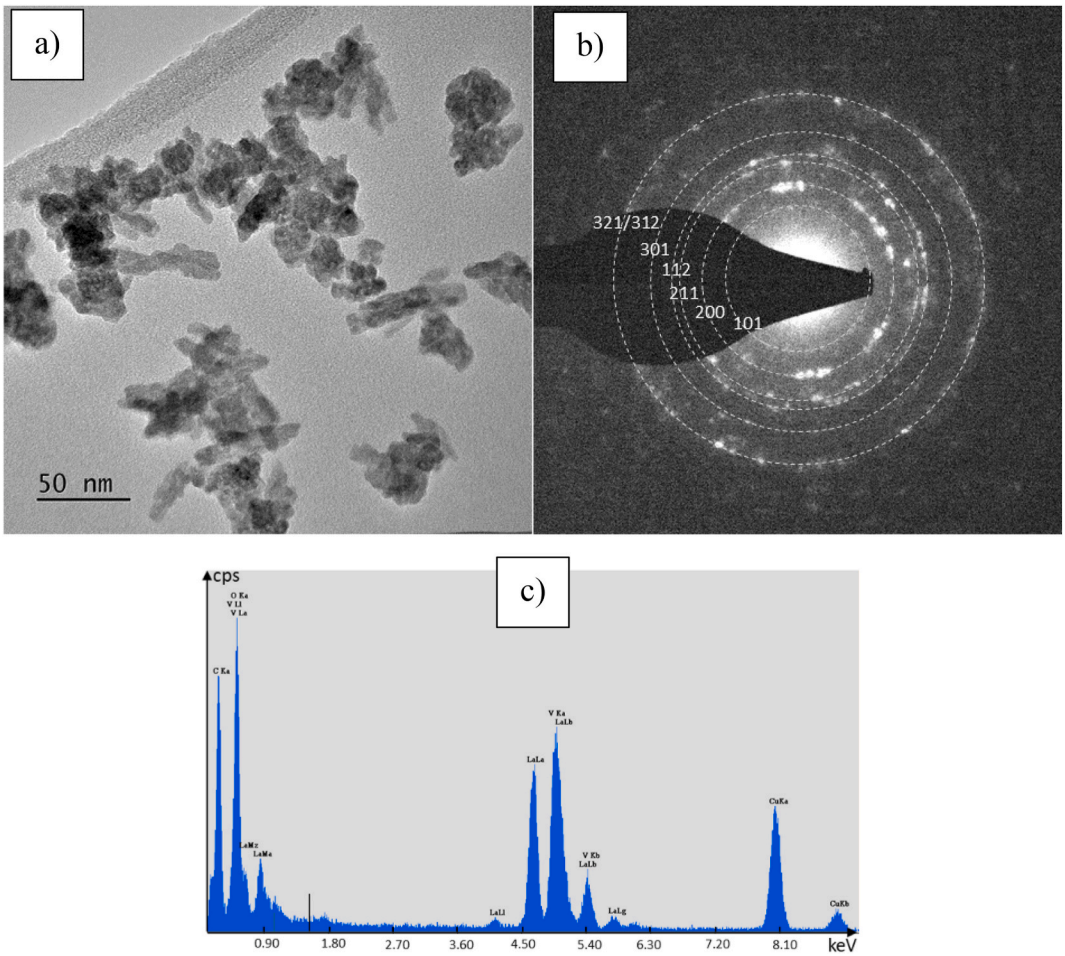

Fig. 3. (a) TEM image (b) electron diffraction pattern and (c) EDS spectra of t-$LaVO_4$.

wherein I_1 and I_2 present the intensities on different times, τ_1 and τ_2 their respective lifetimes. The mean lifetime has been computed by equation (4) [69].

$$\tau_{moy} = \frac{(I_1\tau_1^2 + I_2\tau_2^2)}{(I_1\tau_1 + I_2\tau_2)} \tag{4}$$

The average lifetime of the prepared $LaVO_4$ nanoparticles was 1.108 ns?

4. Photocatalytic activity of $LaVO_4$

4.1. Photolysis and adsorption study

To demonstrate the performance of our $LaVO_4$, it is necessary to evaluate the direct adsorption of the contaminant in the dark. The photolysis study allows the identification of the photocatalytic decomposition in our operational conditions. In this sense, we have done a preliminary study to verify the part of adsorption and photolysis of pollutants (MB). Fig. 5a displays the absorption spectra of MB in the presence of $LaVO_4$. The adsorption process of MB on LVO surface does not exceed **6%** after 3 h of contact indicating a very low adsorption of MB on $LaVO_4$ photocatalyst. The direct photolysis experiment was performed by MB solution with a C_1 of 10 $mg.L^{-1}$ under UV–Vis irradiation. Fig. 5b shows the evolution of MB spectra after 2 h irradiation and only a 4% decomposition of MB is achieved. This confirms the photodegradation in presence of $LaVO_4$ was better than direct photolysis and adsorption process.

4.2. Photocatalytic efficiency and mechanism of t-$LaVO_4$ nanoparticles

Herein, the photocatalytic activity of $LaVO_4$ particles was determined by the photo-degradability considering illumination time of an aqueous MB solution (10 $mg.L^{-1}$). Fig. 6a displays the visible absorption spectra of methylene bleu solution for several time in the

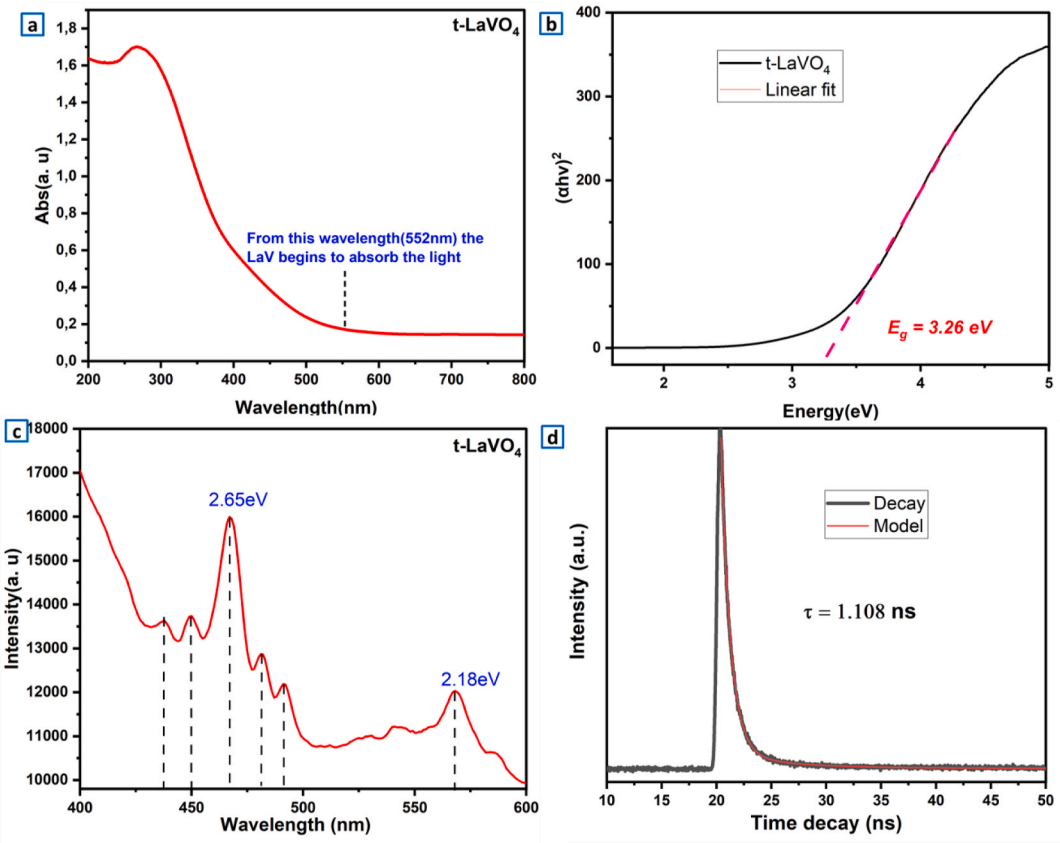

Fig. 4. (a, b) DRS and Tauc's spectra of t-$LaVO_4$ nanoparticles. (c) PL graph of t-$LaVO_4$. (d) TRPL (lifetime-decay) curve of the $LaVO_4$ sample prepared at room temperature.

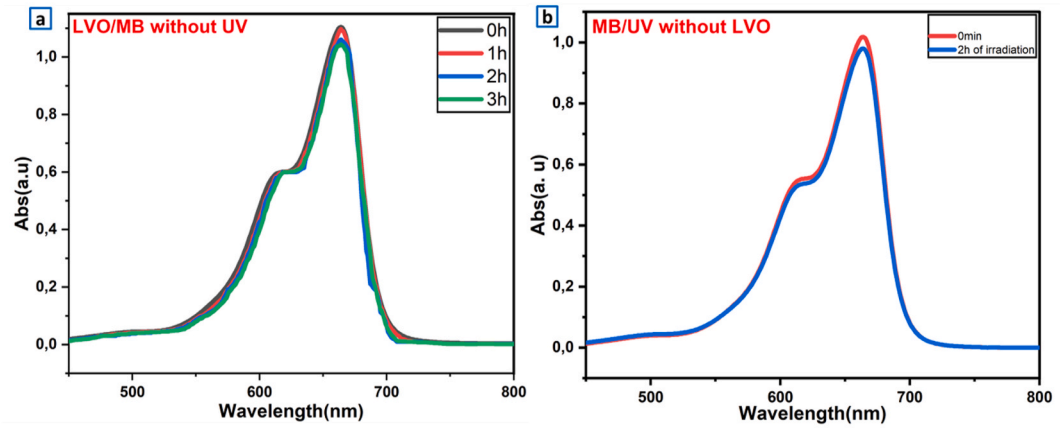

Fig. 5. (a) Absorption spectrum of MB in the presence of $LaVO_4$ catalyst and in the absence of UV illumination. **(b)** photocatalytic decomposition of MB under UV illumination in the absence of $LaVO_4$ particles.

presence of t-$LaVO_4$ NPs. Before any irradiation, the solution should be magnetically agitated for 1 h in darkness to set up the adsorption-desorption equilibrium. The photo-degradation procedure was investigated by measuring the intensity of the absorption bands (664 nm for MB). The intensity of absorption band depends on concentration of selected pollutant. The photo-degradation efficiency was identified by the ratios C_t/C_0 (eq. (4)), in which C_t and C_0 presented the concentrations of $LaVO_4$ at times t and t = 0. The type of kinetics has been evaluated by the relationship in equation (5):

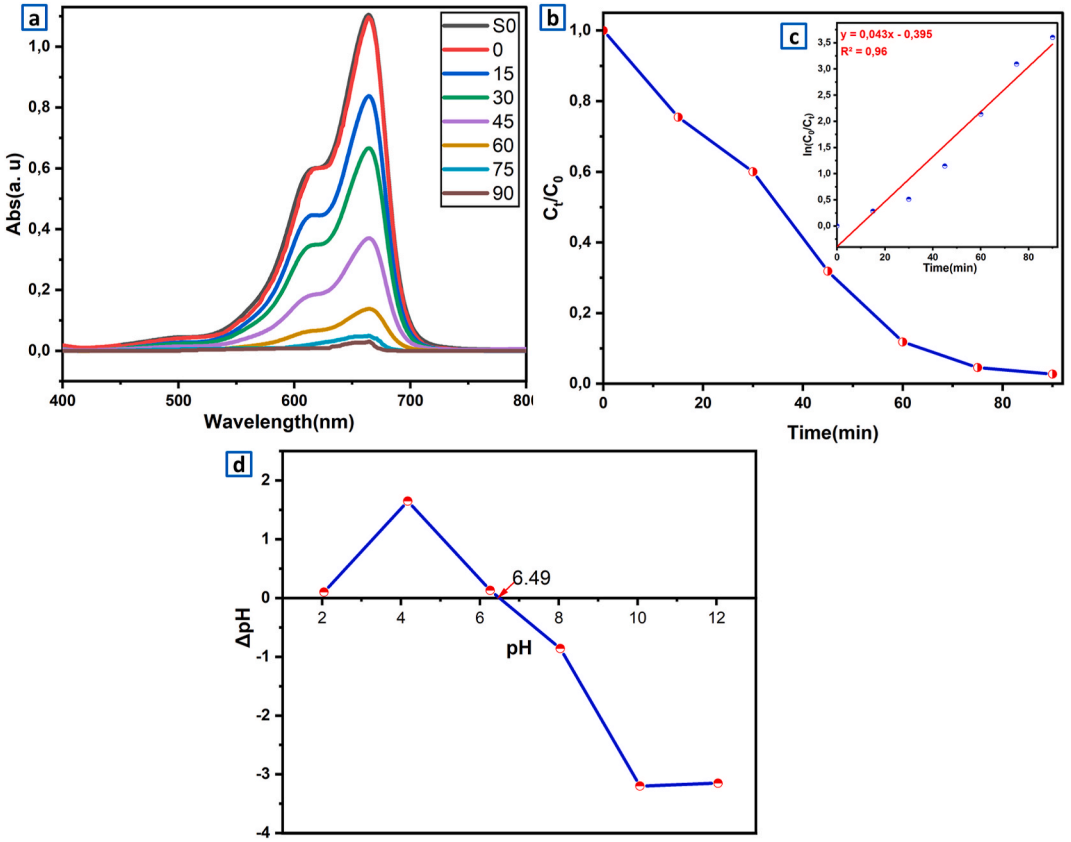

Fig. 6. (a) UV–Vis absorption spectrum of a solution comprising 100 mg of $LaVO_4$ photocatalyst and 10 ppm of pollutant. (b) Variation of the C_t/C_0 report versus time irradiation for the pollutant MB. (c) pseudo-first-order kinetics of the photodecomposition mechanism. (d) Measurement of the zero-point charge of LOV particles: $pH_{pzc} = 6.49$.

$$\ln\frac{C_t}{C_0} = -k_{obs}t \tag{5}$$

In the present relation, k is first order kinetic constant (Langmuir-Hinshelwood model). As can be observed in (Fig. 6a), presented the UV–Vis absorption spectra. It was observed that the absorption peak gradually decreased with increasing irradiation time. They indicated that the reduction in the concentrations of our C_t organic dye is due directly to photocatalytic decomposition. After 90 min of illumination the photocatalytic efficiency obtained by the C_t/C_0 ratio reached 98% (Fig. 6b), this performance is the result of both photolysis and photo-catalysis effects. Fig. 6c illustrates a linear correlation between ln (C_0/C_t) and t which can be easily seen with a rate constant of **0.043 min^{-1}**.

To explain photocatalytic degradation efficiency of MB, we have determined the pH_{pzc} (pH at the zero charge point) Fig. 6d The zero charge point depends on acid-base characteristic of surface material [70]. In our case the tetragonal $LaVO_4$ has PZC at pH 6.49 and MB is a cationic dye. For pHi values under or upon pH_{pzc} the $LaVO_4$ charge surface is positive or negative respectively. This means that the surfaces of $LaVO_4$ can be positively or negatively charged based on the pH of the surrounding environment. In our case the pH of our solution is around 9 which is higher than pH_{pzc}, thus, $LaVO_4$ becomes negatively charged. As a consequence, a high removal efficiency, because of the electrostatic attraction forces occurred between the catalyst surface negatively charged and cationic dye. Moreover, under basic conditions, the efficiency of photo-degradation is more important due to the presence of hydroxyl ions which are necessary for hydroxyl radical's creation. Besides that, this high efficiency is attributed to the specific morphology, which is characterized by small and well crystallized grains of tetragonal phase. It is interesting to mention that the as-prepared photo-catalyst without calcination exhibit good photocatalytic performance by providing small particle size, high specific surface area and more surface sites available for charge transfer [71,72]; these results are in good accordance with the SEM/TEM and XRD results. On the other hand, the optical characteristics of $LaVO_4$, notably its excellent visible light absorption, led us to use a lamp similar to solar irradiation. Furthermore, the photoluminescence study revealed strong emissions in a wide range of colors from blue to red, whose composition was influenced by surface defects, such as oxygen vacancies and variations in the La^{3+} surroundings.

Table 1 gives the photocatalytic efficacy of $LaVO_4$ based catalysts reported in the literature employing different synthesis methods, examined contaminants and light sources. The table shows that the photo-catalyst developed in this study has a similar photocatalytic activity as the other $LaVO_4$-based catalysts discussed in the literature. This activity was explained by the effective separation of the

electron-hole (e^-; h^+) pairs under irradiation.

The following empirical equations (6) and (7) were used to calculate the positions of the valence band (VB) and conduction band (CB) edges of a semiconductor [78]:

$$E_{VB} = X - E^e + 0.5E_g \quad (6)$$

$$E_{CB} = E_{VB} - E_g \quad (7)$$

where, E_{CB} is the conduction band edge, E_{VB} is the valence band edge, X is the electronegativity (5.74 eV) [79], E^e is the energy of the free electrons on the hydrogen scale (approximately 4.5 eV), and E_g is the semiconductor band gap energy (3.26 eV). The calculated E_{CB} and E_{VB} values are (−0.39 and 2.87 eV) For the $LaVO_4$ catalyst.

The calculated valence and conduction bands provided valuable insights into the proposed photocatalytic mechanism, also for the role of superoxide anion radicals in the photo-activity of $LaVO_4$. According to literature, the valence band of $LaVO_4$ is mainly composed of the O2p orbitals, while the conduction band is mainly composed of the V 3d orbitals [80]. Herein, the calculated bandgap of $LaVO_4$ is around 3.26 eV, as shown in Fig. 4b. Based on this information, it is proposed that $LaVO_4$ absorbs visible light and generates electron-hole pairs in the conduction and valence bands, respectively. The photo-generated electrons and holes can react with adsorbed species, such as water and oxygen, to generate superoxide anion radicals and hydroxyl radicals. The calculated valence and conduction bands show that superoxide anion radicals play a major role in the photo-activity of $LaVO_4$.

4.3. Effect of catalyst dosage and pH

The effects of catalyst dosage and pH on the degradation efficiency were studied. As it is known, as property of heterogeneous photo-catalysis, the catalyst dosage influenced the decolorization of wastewater. The photodecomposition of the pollutant increased with the quantity of catalyst [81]. Increasing the amount of photocatalyst effectively causes an excess of active sites on the catalyst surface, leading to creation of –OH radicals that may contribute to the actual discoloration of the pollutant solution. Above a certain threshold of catalyst, the solution turns cloudy, thereby blocking the UV radiation for the reaction to take place, and the rate of degradation begins to decrease [82]. Fig. 7a illustrates the photo-degradation of MB dye at various amounts of $LaVO_4$ photocatalyst. As can be clearly observed, the rate of photo-degradation rises as the quantity of photocatalyst rises. The less amount of photocatalyst (50, 75 mg), the lower the active species formed and therefore a lower rate of degradation was observed, 33 and 73% for 25 and 75 mg respectively during 90 min of irradiation. When the quantity of catalyst is raised to a certain value (150 mg), the capacity of the catalyst to receive photons is saturated and the number of electrons and holes no further increases, so there is no improvement in the degradation rate. When the catalyst amount is great enough, it has a screening and diffusing action on the incident light. It should be noted that the optimum mass for degradation of a 10 ppm concentration of MB is 100 and 125 mg, but from an economic point of view, it is preferable to use a mass of 100 mg. The kinetic study (Fig. 7b and c), showed that the apparent constant increased with the amount of photocatalyst but it started to decrease at 150 mg. The reaction constants were 0.0043, 0.0146, 0.043, 0.0536 and 0,0119 min^{-1} for 50, 75, 100, 125 and 150 mg, respectively. In addition to the effect of the amount of photocatalyst, the pH of the solution seems to play a major role in the photocatalytic process. The effect of pH on the photodecomposition of MB was examined in the pH range 3–9. An essential factor in the photocatalytic processes that take place on the surfaces of particles is the pH of the solution, as it dictates the surface charge characteristics of the photocatalyst [83]. Therefore, pH has an important influence on both the characteristics of dyes and the reaction mechanisms which may participate in dye decomposition, i.e. hydroxyl radical attack, reduction via the electron in CB and direct oxidation by the holes. Fig. 7d shows that the photocatalytic degradation of Methylene Blue increases with increasing pH, confirming the results obtained from the PZC measurement of $LaVO_4$ (Fig. 6d). On the other hand, the increase in pH leads to an increase in OH° radicals, which is beneficial for the photocatalytic process. The photo-degradation of MB is maximal at pH = 9 because it is a cationic dye and the surface of the photocatalyst at this pH point is negative, hence a strong interaction between the negatively charged photocatalyst and the MB of cationic nature. The kinetic study (Fig. 7e and f) showed that the apparent constant increased with the amount of photocatalyst but it started to decrease at 150 mg. The reaction constants were 0.0064, 0.0099, 0.0303 and 0.043 min^{-1} for 3, 5, 7 and 9, respectively.

Table 1
Photocatalytic activity comparison of the $LaVO_4$ photocatalyst with some documented materials.

Catalyst	contaminant examined	Synthesis Method	Operating Conditions (C_0; Light Source)	Degradation Efficiency; Time	Ref
m-$LaVO_4$	MB	Solventless	10^{-5} M, —	82.2%, 90 min	[73]
m-$LaVO_4$	MB	hydrothermal	1.5 10^{-5} M, 400 W metal halide lamp (λ = 510 nm)	91%, 60min	[74]
m-$LaVO_4$/BiOBr	RhB	hydrothermal	3.1 10^{-5} M, 500 W Xe lamp	83.37%, 60min	[75]
t-$LaVO_4$/g-C_3N_4	RhB	hydrothermal	3.1 10^{-5} M, 350 W Xe lamp	99%, 90min	[66]
CNTs/$LaVO_4$	sulfamethazine	hydrothermal	10 10^{-5} M, 400 W metal halide lamp	70%, 90min	[76]
$LaVO_4$/TiO_2	Benzene	Sol-gel	3.2 M, 500 W Xe-arc lamp	57%, 600min	[77]
t-$LaVO_4$	MB	Ambient Synthesis	3.1 10^{-5} M, Philips lamps (300 W)	98%, 90min	This study

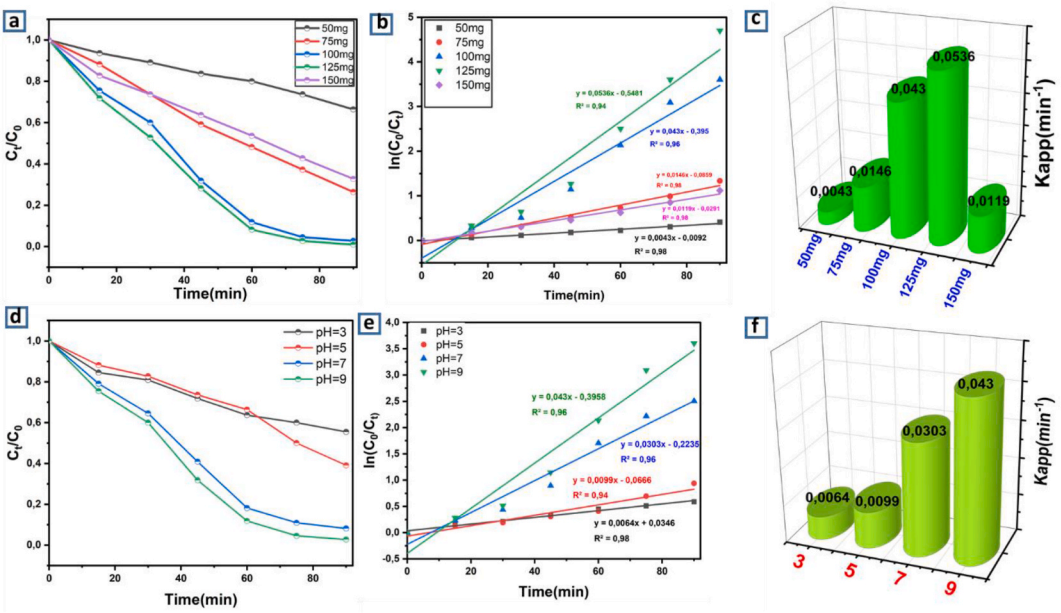

Fig. 7. Photocatalytic degradation of MB in the presence of various quantity of $LaVO_4$ photocatalyst (a, b, c) and different pH of solution (d, e, f).

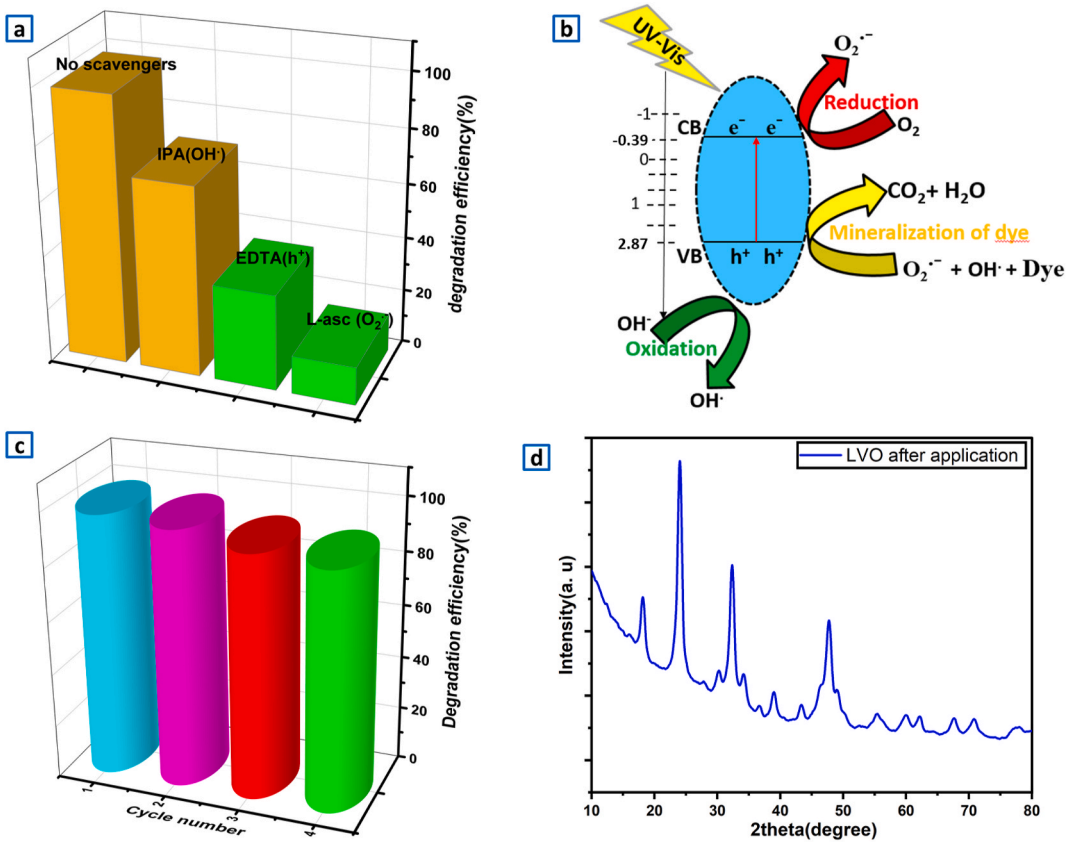

Fig. 8. (a) Photocatalytic degradation of MB by $LaVO_4$ in presence of trapping agents. MB = 10 $mg.L^{-1}$, illumination time = 90 min, scavenger = 4.10^{-3} $mol.L^{-1}$. (b) A schematic diagram illustrating the suggested decomposition mechanism for $LaVO_4$ catalyst. (c) photo-catalyst recycling test. (d) XRD analysis of $LaVO_4$ photo-catalyst after photocatalytic application.

4.4. Trapping test and stability

Radical capture experiments were studied. Isopropanol alcohol (IPA), L-ascorbic acid, ethylene-diamine-tetra-acetic acid disodium (EDTA 2Na) were adopted as h^+, superoxide radical ($\cdot O2^-$) and hydroxyl radical (*OH) scavenger, respectively. Fig. 8a illustrates the effect of the scavengers on the degradation process. The photocatalytic decomposition efficiencies of MB were 98% in the absence of scavengers, while in the presence of IPA, EDTA and L-ascorbic acid, the rate value reduced to 70%, 35.4% and 14.1%, respectively. Therefore, it can be concluded that holes (h^+) and superoxide ($O_2^{\cdot-}$) are essential for the photodecomposition of methylene bleu and hydroxyl radicals ($OH^{\cdot}$) has not greater influence. Similar results confirmed by Samy et al. [74].

According to these obtained results, the proposed mechanism of photocatalytic decomposition is shown in Fig. 8b. The holes (h^+) and electrons (e^-) produced under visible light irradiation react with the molecules presented in the solution such as H_2O, O_2 and OH^- to generate highly active $OH^{\cdot}$ and $O_2^{\cdot-}$ ions respectively. The results obtained by Jilani et al. [84]., confirmed that reactive species break down the MB molecules into smaller entities, that lead to complete mineralization (CO_2+ H_2O). The photogenerated electrons of LVO have a higher reduction potential than $O_2^{\bullet-}/O_2$ (−0.28 eV). As a result, when oxygen molecules (O_2) are adsorbed on the surface of LVO, the released electrons can easily transfer to them, generating $O_2^{\bullet-}$ superoxides. These latter are strong oxidizing species that can degrade organic molecules. Furthermore, it is also possible to produce $OH^{\bullet}$ hydroxyl radicals directly from photogenerated holes. This is because the valence band position of LVO (2.87 eV) is more positive than that of $H_2O/OH^{\bullet}$ (1.99 eV) [85]. Therefore, the holes on the LVO surface can also react with OH^-/H_2O to form free radicals in the photocatalytic reaction. However, $O_2^{\bullet-}$ superoxides have a stronger reduction capacity and can react with H_2O or OH^- to produce $OH^{\bullet}$. This is in agreement with scavengers trapping measurement which shows the predominance of $O_2^{\cdot-}$efficiency followed by the holes.

The stability of $LaVO_4$ was examined by recycling the catalyst for MB decomposition under visible light irradiation. After each reaction, the recovered photo-catalyst was cleaned with deionized water and then was dried for reuse. Fig. 8c presented the test results, which showed a reduction in photo-activity after four successive experiments. The little decrease is probably due to the loss of photo-catalyst during recycling or to the molecules of organic dye MB adsorbed on catalyst surface, as a result of blockage of active sites in process of capturing [86]. XRD analysis Fig. 8d verified that the crystal structure has not altered after the photocatalytic processes.

4.5. MB mineralization via COD analysis

The identification of the Chemical Oxygen Demand (COD) used to determine the level of mineralization of the contaminants after the photocatalytic oxidation. It provides a complementary view of the photocatalytic performance of the photo-catalysts. Fig. 9 illustrates the removal rates of COD for $LaVO_4$ photo-catalyst used in photo-degradation of MB. In terms of COD elimination (Fig. 9a and b), COD removal was 85% after 1 h 30 min of UV–visible illumination for 100 mg of $LaVO_4$, 10 mg/L initial MB concentration at pH 9 and 90 min irradiation time.

This trend is in agreement with the scavenger tests that justify the major role of the O_2^- radicals. So obtaining this COD removal (85%) rate indicates that this photo-catalyst is able to successfully convert MB molecules into CO_2 and H_2O [66].

5. Conclusion

As a summary, lanthanum orthovanadate was prepared successfully by facile co-precipitation method at room temperature. The synthesized $LaVO_4$ crystallizes in tetragonal structure with pin-like nanostructure with a size lower than 14–18 nm. The optical characterization shows a direct gap energy 3.26 eV and an average life time of 1.108 ns, also the particles have interesting photo-luminescence characteristics when they are irradiated by UV light.

The photocatalytic activity analyses indicated that the $LaVO_4$ prepared to have good photocatalytic activity, degradation of the methylene blue solution (99%) of concentration 10 $mg.L^{-1}$ during 90 min of irradiation. The enhanced activity could be attributed to the nanometric size of the particles which offer more active sites as well as its capacities to absorb light in the visible range. Radical trapping investigations showed that superoxide and holes species contributed to the decomposition of MB. The reusability of $LaVO_4$ samples was evaluated in four consecutive runs indicating great stability of the photocatalyst after long photocatalytic reaction periods.

Author contribution statement

Safia Lotfi, Mohamed El ouardi: Conceived and designed the experiments; Performed the experiments; Analyzed and interpreted the data; Wrote the paper.

Hassan Ait Ahsaine: Conceived and designed the experiments; Analyzed and interpreted the data; Contributed reagents, materials, analysis tools or data; Wrote the paper.

Veronique Madigou: Performed the experiments; Analyzed and interpreted the data; Wrote the paper.

Amal BaQais: Analysis tools or data; Interpreted the data; Wrote the paper.

Abderrazzak Assani, Mohamed Saadi: Conceived and designed the experiments; Analyzed and interpreted the data; Wrote the paper.

Madjid Arab: Conceived and designed the experiments; Analyzed and interpreted the data; Wrote the paper.

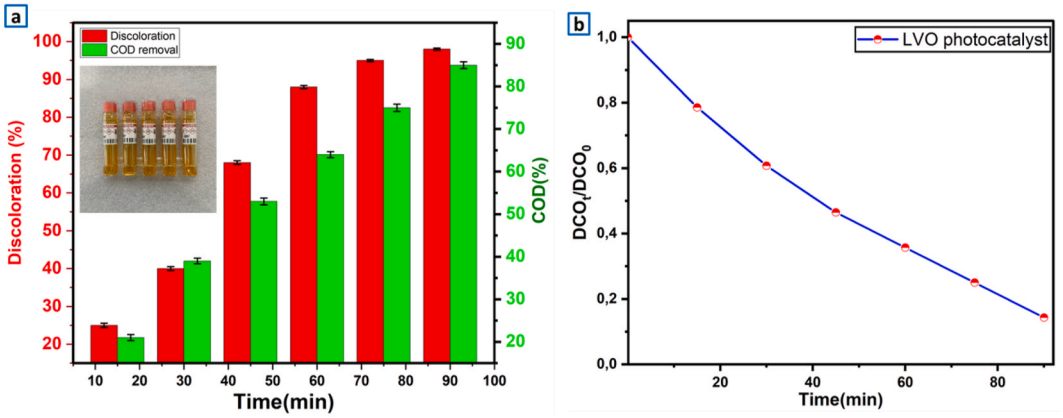

Fig. 9. a, b) Analysis of chemical oxygen demand removal versus time using $LaVO_4$ photo-catalyst, pH = 9, photo-catalyst mass = 100 mg, [MB] = 10 mg/L, irradiation time 90 min.

Data availability statement

Data will be made available on request.

Declaration of competing interest

The authors declare that they have no known competing financial interests or personal relationships that could have appeared to influence the work reported in this paper

Acknowledgements

Safia Lotfi thanks the support of CNRST (Centre National pour la Recherche Scientifique et Technique) in the Excellence Research Scholarships Program. The authors are thankful to the faculty of Science, Mohammed V University in Rabat, Morocco. Authors are grateful for the support of the IM2NP laboratory at University of Toulon, France for providing the characterization research facilities. Authors thanks also the Princess Nourah Bint Abdulrahman university researchers supporting project (PNURSP2023R230), Princess Nourah Bint Abdulrahman university, Riyadh,Saudi Arabia.

References

[1] A. Amjlef, S. Khrach, A. Ait El Fakir, S. Farsad, S. Et-Taleb, N. El Alem, Adsorptive properties investigation of natural sand as adsorbent for methylene blue removal from contaminated water, Nanotechnol. Environ. Eng. 6 (2021) 26, https://doi.org/10.1007/s41204-021-00119-y.
[2] A.N. Saeid Taghavi Fardood, Farzaneh Moradnia, Siamak Heidarzadeh, Green synthesis, characterization, photocatalytic and antibacterial activities of copper oxide nanoparticles of copper oxide nanoparticles, Nano Res. 8 (2023) 134–140, https://doi.org/10.22036/ncr.2023.02.006.
[3] Z. Li, J. Mei, L. Bai, Synthesis of C_3N_4-decorated ZnO and Ag/ZnO nanoparticles via calcination of ZIF-8 and melamine for photocatalytic removal of methyl orange, Chem. Pap. 73 (2019) 883–889, https://doi.org/10.1007/s11696-018-0656-7.
[4] B. Akhsassi, A. Bouddouch, Y. Naciri, B. Bakiz, A. Taoufyq, C. Favotto, S. Villain, F. Guinneton, A. Benlhachemi, Enhanced photocatalytic activity of $Zn_3(PO_4)_2$/ZnO composite semiconductor prepared by different methods, Chem. Phys. Lett. 783 (2021), 139046, https://doi.org/10.1016/j.cplett.2021.139046.
[5] L.A. Shah, M. Sayed, M. Fayaz, I. Bibi, M. Nawaz, M. Siddiq, Ag-loaded thermo-sensitive composite microgels for enhanced catalytic reduction of methylene blue, Nanotechnol. Environ. Eng. 2 (2017) 14, https://doi.org/10.1007/s41204-017-0026-7.
[6] P. Raizada, A. Sudhaik, P. Singh, Photocatalytic water decontamination using graphene and ZnO coupled photocatalysts: a review, Mater. Sci. Energy Technol. 2 (2019) 509–525, https://doi.org/10.1016/j.mset.2019.04.007.
[7] S. Taghavi Fardood, F. Moradnia, R. Forootan, R. Abbassi, S. Jalalifar, A. Ramazani, M. Sillanpää, Facile green synthesis, characterization and visible light photocatalytic activity of MgFe2O4@CoCr2O4 magnetic nanocomposite, J. Photochem. Photobiol. Chem. 423 (2022), 113621, https://doi.org/10.1016/j.jphotochem.2021.113621.
[8] A. Karim, B. Achiou, A. Bouazizi, A. Aaddane, M. Ouammou, M. Bouziane, J. Bennazha, S. Alami Younssi, Development of reduced graphene oxide membrane on flat Moroccan ceramic pozzolan support. Application for soluble dyes removal, J. Environ. Chem. Eng. 6 (2018) 1475–1485, https://doi.org/10.1016/j.jece.2018.01.055.
[9] H. Liu, J. Zhang, M. Lu, L. Liang, H. Zhang, J. Wei, Biosynthesis based membrane filtration coupled with iron nanoparticles reduction process in removal of dyes, Chem. Eng. J. 387 (2020), 124202, https://doi.org/10.1016/j.cej.2020.124202.
[10] A. Imgharn, H. Ighnih, A. Hsini, Y. Naciri, M. Laabd, H. Kabli, M. Elamine, R. Lakhmiri, B. Souhail, A. Albourine, Synthesis and characterization of polyaniline-based biocomposites and their application for effective removal of Orange G dye using adsorption in dynamic regime, Chem. Phys. Lett. 778 (2021), 138811, https://doi.org/10.1016/j.cplett.2021.138811.
[11] Z. Anfar, A. Amedlous, A.A. El Fakir, M. Zbair, H. Ait Ahsaine, A. Jada, N. El Alem, High extent mass recovery of alginate hydrogel beads network based on immobilized bio-sourced porous carbon@Fe3O4-NPs for organic pollutants uptake, Chemosphere 236 (2019), 124351, https://doi.org/10.1016/j.chemosphere.2019.124351.
[12] D.D. Manholer, M.T.F. de Souza, E. Ambrosio, T.K.F. de Souza Freitas, H.C.L. Geraldino, J.C. Garcia, Coagulation/flocculation of textile effluent using a natural coagulant extracted from Dillenia indica, Water Sci. Technol. 80 (2019) 979–988, https://doi.org/10.2166/wst.2019.342.
[13] C.Y. Teh, P.M. Budiman, K.P.Y. Shak, T.Y. Wu, Recent advancement of coagulation–flocculation and its application in wastewater treatment, Ind. Eng. Chem. Res. 55 (2016) 4363–4389, https://doi.org/10.1021/acs.iecr.5b04703.

[14] M.T. Selim, S.S. Salem, A.A. Mohamed, M.S. El-Gamal, M.F. Awad, A. Fouda, Biological treatment of real textile effluent using Aspergillus flavus and Fusarium oxysporium and their consortium along with the evaluation of their phytotoxicity, J. Fungi 7 (2021) 193, https://doi.org/10.3390/jof7030193.

[15] A. Sharma, Z. Syed, U. Brighu, A.B. Gupta, C. Ram, Adsorption of textile wastewater on alkali-activated sand, J. Clean. Prod. 220 (2019) 23–32, https://doi.org/10.1016/j.jclepro.2019.01.236.

[16] F. Moradnia, S. Taghavi Fardood, A. Ramazani, V.K. Gupta, Green synthesis of recyclable MgFeCrO4 spinel nanoparticles for rapid photodegradation of direct black 122 dye, J. Photochem. Photobiol. Chem. 392 (2020), 112433, https://doi.org/10.1016/j.jphotochem.2020.112433.

[17] S. Lotfi, M. El Ouardi, H.A. Ahsaine, A. Assani, Recent progress on the synthesis, morphology and photocatalytic dye degradation of BiVO 4 photocatalysts: a review, Catal. Rev. (2022) 1–45, https://doi.org/10.1080/01614940.2022.2057044.

[18] W. Nachit, H. Ait Ahsaine, Z. Ramzi, S. Touhtouh, I. Goncharova, K. Benkhouja, Photocatalytic activity of anatase-brookite TiO2 nanoparticles synthesized by sol gel method at low temperature, Opt. Mater. 129 (2022), 112256, https://doi.org/10.1016/j.optmat.2022.112256.

[19] Y. Wu, Z. Gao, X. Sun, H. Cai, X. Wu, Photo-degradation organic dyes by Sb-based organic-inorganic hybrid ferroelectrics, J. Environ. Sci. 101 (2021) 145–155, https://doi.org/10.1016/j.jes.2020.08.014.

[20] R. Zhang, Y. Ma, W. Lan, D.E. Sameen, S. Ahmed, J. Dai, W. Qin, S. Li, Y. Liu, Enhanced photocatalytic degradation of organic dyes by ultrasonic-assisted electrospray TiO2/graphene oxide on polyacrylonitrile/β-cyclodextrin nanofibrous membranes, Ultrason. Sonochem. 70 (2021), 105343, https://doi.org/10.1016/j.ultsonch.2020.105343.

[21] Y. Naciri, H. Ait Ahsaine, A. Chennah, A. Amedlous, A. Taoufyq, B. Bakiz, M. Ezahri, S. Villain, A. Benlhachemi, Facile synthesis, characterization and photocatalytic performance of Zn3(PO4)2 platelets toward photodegradation of Rhodamine B dye, J. Environ. Chem. Eng. 6 (2018) 1840–1847, https://doi.org/10.1016/j.jece.2018.02.009.

[22] H. Ait Ahsaine, M. Ezahri, A. Benlhachemi, B. Bakiz, S. Villain, F. Guinneton, J.-R. Gavarri, Novel Lu-doped Bi2WO6 nanosheets: synthesis, growth mechanisms and enhanced photocatalytic activity under UV-light irradiation, Ceram. Int. 42 (2016) 8552–8558, https://doi.org/10.1016/j.ceramint.2016.02.082.

[23] O. Yayapao, T. Thongtem, A. Phuruangrat, S. Thongtem, Synthesis and characterization of highly efficient Gd doped ZnO photocatalyst irradiated with ultraviolet and visible radiations, Mater. Sci. Semicond. Process. 39 (2015) 786–792, https://doi.org/10.1016/j.mssp.2015.06.039.

[24] F. Moradnia, S. Taghavi Fardood, A. Ramazani, B. Min, S.W. Joo, R.S. Varma, Magnetic Mg0.5Zn0.5FeMnO4 nanoparticles: green sol-gel synthesis, characterization, and photocatalytic applications, J. Clean. Prod. 288 (2021), 125632, https://doi.org/10.1016/j.jclepro.2020.125632.

[25] Y. Naciri, A. Hsini, Z. Ajmal, J.A. Navío, B. Bakiz, A. Albourine, M. Ezahri, A. Benlhachemi, Recent progress on the enhancement of photocatalytic properties of BiPO4 using π–conjugated materials, Adv. Colloid Interface Sci. 280 (2020), 102160, https://doi.org/10.1016/j.cis.2020.102160.

[26] J.-M. Herrmann, Heterogeneous photocatalysis: fundamentals and applications to the removal of various types of aqueous pollutants, Catal. Today 53 (1999) 115–129, https://doi.org/10.1016/S0920-5861(99)00107-8.

[27] H. Ait ahsaine, M. Ezahri, A. Benlhachemi, B. Bakiz, S. Villain, J.-C. Valmalette, F. Guinneton, M. Arab, J.-R. Gavarri, Structural, vibrational study and UV photoluminescence properties of the system $Bi_{(2-x)}$ $Lu_{(x)}WO_6$ ($0.1 \leq x \leq 1$), RSC Adv. 5 (2015) 96242–96252, https://doi.org/10.1039/C5RA19424E.

[28] H. Ait Ahsaine, A. El jaouhari, A. Slassi, M. Ezahri, A. Benlhachemi, B. Bakiz, F. Guinneton, J.-R. Gavarri, Electronic band structure and visible-light photocatalytic activity of Bi_2WO_6: elucidating the effect of lutetium doping, RSC Adv. 6 (2016) 101105–101114, https://doi.org/10.1039/C6RA22669H.

[29] H. Ait Ahsaine, UV-light photocatalytic properties of the bismuth lutetium tungstate system Bi_{2-x} Lu_xWO_6 ($0 \leq x \leq 1$), Mater. Lett. 276 (2020), 128221, https://doi.org/10.1016/j.matlet.2020.128221.

[30] P. Siriwong, T. Thongtem, A. Phuruangrat, S. Thongtem, Hydrothermal synthesis, characterization, and optical properties of wolframite $ZnWO_4$ nanorods, CrystEngComm 13 (2011) 1564–1569, https://doi.org/10.1039/C0CE00402B.

[31] S. Pinchujit, A. Phuruangrat, S. Wannapop, T. Sakhon, B. Kuntalue, T. Thongtem, S. Thongtem, Synthesis and characterization of heterostructure Pt/Bi_2WO_6 nanocomposites with enhanced photodegradation efficiency induced by visible radiation, Solid State Sci. 134 (2022), 107064, https://doi.org/10.1016/j.solidstatesciences.2022.107064.

[32] A. Phuruangrat, S. Wannapop, T. Sakhon, B. Kuntalue, T. Thongtem, S. Thongtem, Characterization and photocatalytic properties of BiVO4 synthesized by combustion method, J. Mol. Struct. 1274 (2023), 134420, https://doi.org/10.1016/j.molstruc.2022.134420.

[33] H.A. Ahsaine, A. Slassi, Y. Naciri, A. Chennah, C. Jaramillo-Páez, Z. Anfar, M. Zbair, A. Benlhachemi, J.A. Navío, Photo/electrocatalytic properties of nanocrystalline ZnO and La–doped ZnO: combined DFT fundamental semiconducting properties and experimental study, ChemistrySelect 3 (2018) 7778–7791, https://doi.org/10.1002/slct.201801729.

[34] S. Kumar, R.D. Kaushik, L.P. Purohit, Novel ZnO tetrapod-reduced graphene oxide nanocomposites for enhanced photocatalytic degradation of phenolic compounds and MB dye, J. Mol. Liq. 327 (2021), 114814, https://doi.org/10.1016/j.molliq.2020.114814.

[35] A. Mobeen, C. Maria Magdalane, S.K. Jasmine Shahina, D. Lakshmi, R. Sundaram, G. Ramalingam, A. Raja, J. Madhavan, D. Letsholathebe, A.K.H. Bashir, M. Maaza, K. Kaviyarasu, Investigation on antibacterial and photocatalytic degradation of Rhodamine-B dye under visible light irradiation by titanium molybdate nanoparticles prepared via microwave method, Surface. Interfac. 17 (2019), 100381, https://doi.org/10.1016/j.surfin.2019.100381.

[36] M. El Ouardi, A. El aouni, H. Ait Ahsaine, M. Zbair, A. BaQais, M. Saadi, ZIF-8 metal organic framework composites as hydrogen evolution reaction photocatalyst: a review of the current state, Chemosphere 308 (2022), 136483, https://doi.org/10.1016/j.chemosphere.2022.136483.

[37] K. Bhuvaneswari, G. Palanisamy, T. Pazhanivel, T. Maiyalagan, P. Shanmugam, A.N. Grace, In-situ development of metal organic frameworks assisted ZnMgAl layered triple hydroxide 2D/2D hybrid as an efficient photocatalyst for organic dye degradation, Chemosphere 270 (2021), 128616, https://doi.org/10.1016/j.chemosphere.2020.128616.

[38] T. Li, L. Zhao, Y. He, J. Cai, M. Luo, J. Lin, Synthesis of g-C_3N_4/$SmVO_4$ composite photocatalyst with improved visible light photocatalytic activities in RhB degradation, Appl. Catal. B Environ. 129 (2013) 255–263, https://doi.org/10.1016/j.apcatb.2012.09.031.

[39] G. Lu, X. Zou, F. Wang, H. Wang, W. Li, Facile fabrication of $CeVO_4$ microspheres with efficient visible-light photocatalytic activity, Mater. Lett. 195 (2017) 168–171, https://doi.org/10.1016/j.matlet.2017.02.128.

[40] R. Yang, Y. Zhang, Y. Fan, R. Wang, R. Zhu, Y. Tang, Z. Yin, Z. Zeng, $InVO_4$-based photocatalysts for energy and environmental applications, Chem. Eng. J. 428 (2022), 131145, https://doi.org/10.1016/j.cej.2021.131145.

[41] K.P. Thaba, M.M. Mphahlele-Makgwane, P.I. Kyesmen, M. Diale, P.G.L. Baker, P.R. Makgwane, Composition-dependent structure evolution of $FeVO_4$ nano-oxide and its visible-light photocatalytic activity for degradation of methylene blue, Colloids Surf. A Physicochem. Eng. Asp. 633 (2022), 127856, https://doi.org/10.1016/j.colsurfa.2021.127856.

[42] Y. He, Y. Wang, L. Zhao, X. Wu, Y. Wu, Preparation, characterization and activity evaluation of V_2O_5–$LaVO_4$ composites under visible light irradiation, J. Mol. Catal. Chem. 337 (2011) 61–67, https://doi.org/10.1016/j.molcata.2011.01.015.

[43] Ü. Kersen, R.L. Keiski, Preliminary study on the selective oxidation of H_2S over $LaVO_4$ and $Fe_2(MoO_4)_3$ oxides, produced by a solvothermal method, Catal. Commun. 10 (2009) 1039–1042, https://doi.org/10.1016/j.catcom.2008.12.052.

[44] X. Zou, X. Li, Q. Zhao, S. Liu, Synthesis of $LaVO_4$/TiO_2 heterojunction nanotubes by sol–gel coupled with hydrothermal method for photocatalytic air purification, J. Colloid Interface Sci. 383 (2012) 13–18, https://doi.org/10.1016/j.jcis.2012.05.051.

[45] L. Sun, X. Zhao, Y. Li, P. Li, H. Sun, X. Cheng, W. Fan, First-principles studies of electronic, optical, and vibrational properties of $LaVO_4$ polymorph, J. Appl. Phys. 108 (2010), 093519, https://doi.org/10.1063/1.3499308.

[46] F. Zhang, G. Li, W. Zhang, Y.L. Yan, Phase-Dependent enhancement of the green-emitting upconversion fluorescence in $LaVO_4$:Yb_{3+}, Er_{3+}, Inorg. Chem. 54 (2015) 7325–7334, https://doi.org/10.1021/acs.inorgchem.5b00851.

[47] W. Fan, Y. Bu, X. Song, S. Sun, X. Zhao, Selective synthesis and luminescent properties of monazite- and zircon-type $LaVO_4$:ln (ln = Eu, Sm, and Dy) nanocrystals, Cryst. Growth Des. 7 (2007) 2361–2366, https://doi.org/10.1021/cg060807o.

[48] Y. Oka, T. Yao, N. Yamamoto, Hydrothermal synthesis of lanthanum vanadates: synthesis and crystal structures of zircon-type $LaVO_4$ and a new compound LaV_3O_9, J. Solid State Chem. 152 (2000) 486–491, https://doi.org/10.1006/jssc.2000.8717.

[49] C.-J. Jia, L.-D. Sun, L.-P. You, X.-C. Jiang, F. Luo, Y.-C. Pang, C.-H. Yan, Selective synthesis of monazite- and zircon-type $LaVO_4$ nanocrystals, J. Phys. Chem. B 109 (2005) 3284–3290, https://doi.org/10.1021/jp045967u.

[50] G. Herrera, E. Chavira, J. Jiménez-Mier, A. Ordoñez, E. Fregoso-Israel, L. Baños, E. Bucio, J. Guzmán, O. Novelo, C. Flores, Structural and morphology comparison between m-$LaVO_4$ and $LaVO_3$ compounds prepared by sol–gel acrylamide polymerization and solid state reaction, J. Alloys Compd. 479 (2009) 511–519, https://doi.org/10.1016/j.jallcom.2008.12.146.

[51] K.-T. Li, C.-H. Huang, Selective oxidation of hydrogen sulfide to sulfur over $LaVO_4$ catalyst: promotional effect of antimony oxide addition, Ind. Eng. Chem. Res. 45 (2006) 7096–7100, https://doi.org/10.1021/ie060384n.

[52] S.Y. Zhong, H.S. Ye, J.Q. Jiang, Q. Yang, P.S. Tang, Preparation of $LaVO_4$ by microwave process and its photocatalytic activity, Mater. Sci. Forum 852 (2016) 538–541, https://doi.org/10.4028/www.scientific.net/MSF.852.538.

[53] I. Shafiq, M. Hussain, S. Shafique, R. Rashid, P. Akhter, A. Ahmed, J.-K. Jeon, Y.-K. Park, Oxidative desulfurization of refinery diesel pool fractions using $LaVO_4$ photocatalyst, J. Ind. Eng. Chem. 98 (2021) 283–288, https://doi.org/10.1016/j.jiec.2021.03.040.

[54] W. Fan, X. Song, S. Sun, X. Zhao, Microemulsion-mediated hydrothermal synthesis and characterization of zircon-type $LaVO_4$ nanowires, J. Solid State Chem. 180 (2007) 284–290, https://doi.org/10.1016/j.jssc.2006.10.019.

[55] Y. Oka, T. Yao, N. Yamamoto, Hydrothermal synthesis of lanthanum vanadates: synthesis and crystal structures of zircon-type $LaVO_4$ and a new compound LaV_3O_9, J. Solid State Chem. 152 (2000) 486–491, https://doi.org/10.1006/jssc.2000.8717.

[56] I. Shafiq, M. Hussain, R. Rashid, S. Shafique, P. Akhter, W. Yang, A. Ahmed, Z. Nawaz, Y.-K. Park, Development of hierarchically porous $LaVO_4$ for efficient visible-light-driven photocatalytic desulfurization of diesel, Chem. Eng. J. 420 (2021), 130529, https://doi.org/10.1016/j.cej.2021.130529.

[57] M.T. Kiani, A. Ramazani, S. Taghavi Fardood, Green synthesis and characterization of $Ni_{0.25}Zn_{0.75}Fe_2O_4$ magnetic nanoparticles and study of their photocatalytic activity in the degradation of aniline, Appl. Organomet. Chem. 37 (2023), https://doi.org/10.1002/aoc.7053.

[58] S. Moradi, S. Taghavi Fardood, A. Ramazani, Green synthesis and characterization of magnetic $NiFe_2O_4$@ZnO nanocomposite and its application for photocatalytic degradation of organic dyes, J. Mater. Sci. Mater. Electron. 29 (2018) 14151–14160, https://doi.org/10.1007/s10854-018-9548-4.

[59] F. Moradnia, S. Taghavi Fardood, A. Ramazani, S. Osali, I. Abdolmaleki, Green sol–gel synthesis of $CoMnCrO_4$ spinel nanoparticles and their photocatalytic application, Micro & Nano Lett. 15 (2020) 674–677, https://doi.org/10.1049/mnl.2020.0189.

[60] J. Ma, Q. Wu, Y. Ding, Selective synthesis of monoclinic and tetragonal phase LaVO4 nanorods via oxides-hydrothermal route, J. Nanoparticle Res. 10 (2008) 775–786, https://doi.org/10.1007/s11051-007-9312-9.

[61] B. Eskandari Azar, A. Ramazani, S. Taghavi Fardood, A. Morsali, Green synthesis and characterization of $ZnAl_2O_4$@ZnO nanocomposite and its environmental applications in rapid dye degradation, Optik 208 (2020), 164129, https://doi.org/10.1016/j.ijleo.2019.164129.

[62] P. Gangwar, M. Pandey, S. Sivakumar, R.G.S. Pala, G. Parthasarathy, Increased loading of Eu_{3+} ions in monazite $LaVO_4$ nanocrystals via pressure-driven phase transitions, Cryst. Growth Des. 13 (2013) 2344–2349, https://doi.org/10.1021/cg3018908.

[63] X. Cheng, D. Guo, S. Feng, K. Yang, Y. Wang, Y. Ren, Y. Song, Structure and stability of monazite- and zircon-type $LaVO_4$ under hydrostatic pressure, Opt. Mater. 49 (2015) 32–38, https://doi.org/10.1016/j.optmat.2015.08.011.

[64] V.P. Filonenko, M. Sundberg, P.-E. Werner, I.P. Zibrov, Structure of a high-pressure phase of vanadium pentoxide, β-V_2O_5, Acta Crystallogr. Sect. B Struct. Sci. 60 (2004) 375–381, https://doi.org/10.1107/S0108768104012881.

[65] J. Tauc, R. Grigorovici, A. Vancu, Optical properties and electronic structure of amorphous germanium, Phys. Status Solidi 15 (1966) 627–637, https://doi.org/10.1002/pssb.19660150224.

[66] Y. He, J. Cai, L. Zhang, X. Wang, H. Lin, B. Teng, L. Zhao, W. Weng, H. Wan, M. Fan, Comparing two new composite photocatalysts, t -$LaVO_4$/g-C_3N_4 and m-$LaVO_4$/g-C_3N_4, for their structures and performances, Ind. Eng. Chem. Res. 53 (2014) 5905–5915, https://doi.org/10.1021/ie4043856.

[67] L. Xue, Y. Li-Li, Y. Li-Na, G. Qing-Feng, Y. Yong-Sheng, Z. Han, Controllable synthesis and photocatalytic activity of spherical, flowerlike and threadlike bismuth vanadates, Acta Phys. Chim. Sin. 29 (2013) 1771–1777, https://doi.org/10.3866/PKU.WHXB201305131.

[68] F. Wang, H. Zhang, L. Liu, B. Shin, F. Shan, Synthesis, surface properties and optical characteristics of CuV_2O_6 nanofibers, J. Alloys Compd. 672 (2016) 229–237, https://doi.org/10.1016/j.jallcom.2016.02.089.

[69] H. Wang, M. Yu, C.K. Lin, J. Lin, Core–shell structured SiO_2@YVO_4:Dy_{3+}/Sm_{3+} phosphor particles: sol–gel preparation and characterization, J. Colloid Interface Sci. 300 (2006) 176–182, https://doi.org/10.1016/j.jcis.2006.03.052.

[70] A. Bouddouch, B. Akhsassi, E. Amaterz, B. Bakiz, A. Taoufyq, S. Villain, F. Guinneton, A. El Aamrani, J.-R. Gavarri, A. Benlhachemi, Photodegradation under UV light irradiation of various types and systems of organic pollutants in the presence of a performant BiPO4 photocatalyst, Catalysts 12 (2022) 691, https://doi.org/10.3390/catal12070691.

[71] A.C. Dodd, A.J. McKinley, M. Saunders, T. Tsuzuki, Effect of particle size on the photocatalytic activity of nanoparticulate zinc oxide, J. Nanoparticle Res. 8 (2006) 43–51, https://doi.org/10.1007/s11051-005-5131-z.

[72] A. Sivakumar, B. Murugesan, A. Loganathan, P. Sivakumar, A review on decolourisation of dyes by photodegradation using various bismuth catalysts, J. Taiwan Inst. Chem. Eng. 45 (2014) 2300–2306, https://doi.org/10.1016/j.jtice.2014.07.003.

[73] V. Sivakumar, R. Suresh, K. Giribabu, V. Narayanan, Solventless synthesis of m-LaVO4 photocatalyst for the degradation of methylene blue and textile effluent, J. Mater. Sci. Mater. Electron. 28 (2017) 4014–4019, https://doi.org/10.1007/s10854-016-6014-z.

[74] M. Samy, M.G. Ibrahim, M. Gar Alalm, M. Fujii, Modeling and optimization of photocatalytic degradation of methylene blue using lanthanum vanadate, Mater. Sci. Forum 1008 (2020) 97–103, https://doi.org/10.4028/www.scientific.net/MSF.1008.97.

[75] J. Ma, S. Liu, G. Qi, Synthesis of m-$LaVO_4$/BiOBr composite photocatalysts and their photocatalytic performance under visible light, Mater. Res. Bull. 95 (2017) 146–151, https://doi.org/10.1016/j.materresbull.2017.07.032.

[76] M. Samy, M.G. Ibrahim, M. Gar Alalm, M. Fujii, Effective photocatalytic degradation of sulfamethazine by CNTs/$LaVO_4$ in suspension and dip coating modes, Sep. Purif. Technol. 235 (2020), 116138, https://doi.org/10.1016/j.seppur.2019.116138.

[77] H. Huang, D. Li, Q. Lin, W. Zhang, Y. Shao, Y. Chen, M. Sun, X. Fu, Efficient degradation of benzene over $LaVO_4$/TiO_2 nanocrystalline heterojunction photocatalyst under visible light irradiation, Environ. Sci. Technol. 43 (2009) 4164–4168, https://doi.org/10.1021/es900393h.

[78] C. Zhang, K. Yu, Y. Feng, Y. Chang, T. Yang, Y. Xuan, D. Lei, L.-L. Lou, S. Liu, Novel 3DOM-$SrTiO_3$/Ag/Ag_3PO_4 ternary Z-scheme photocatalysts with remarkably improved activity and durability for contaminant degradation, Appl. Catal. B Environ. 210 (2017) 77–87, https://doi.org/10.1016/j.apcatb.2017.03.058.

[79] I.A. Mkhalid, R.M. Mohamed, M. Alhaddad, A. Basaleh, L.A. Al-Hajji, A.A. Ismail, Construction of mesoporous lanthanum orthovanadate/carbon nitride heterojunction photocatalyst for the mineralization of trichloroethylene, Ceram. Int. 48 (2022) 14899–14912, https://doi.org/10.1016/j.ceramint.2022.02.028.

[80] S.Y. Zhong, H.S. Ye, J.Q. Jiang, Q. Yang, P.S. Tang, Preparation of LaVO4 by microwave process and its photocatalytic activity, Mater. Sci. Forum 852 (2016) 538–541, https://doi.org/10.4028/www.scientific.net/MSF.852.538.

[81] M.R. Al-Mamun, S. Kader, M.S. Islam, M.Z.H. Khan, Photocatalytic activity improvement and application of UV-TiO2 photocatalysis in textile wastewater treatment: a review, J. Environ. Chem. Eng. 7 (2019), 103248, https://doi.org/10.1016/j.jece.2019.103248.

[82] A. Elaouni, M.E. Ouardi, M. Zbair, A. BaQais, M. Saadi, H.A. Ahsaine, ZIF-8 metal organic framework materials as a superb platform for the removal and photocatalytic degradation of organic pollutants: a review, RSC Adv. 12 (2022) 31801–31817, https://doi.org/10.1039/D2RA05717D.

[83] M. Desseigne, N. Dirany, V. Chevallier, M. Arab, Shape dependence of photosensitive properties of WO_3 oxide for photocatalysis under solar light irradiation, Appl. Surf. Sci. 483 (2019) 313–323, https://doi.org/10.1016/j.apsusc.2019.03.269.

[84] A. Jilani, A.A. Melaibari, MoS2-Cu/CuO@graphene heterogeneous photocatalysis for enhanced photocatalytic degradation of MB from water, Polymers 14 (2022) 3259, https://doi.org/10.3390/polym14163259.

[85] D. Wang, L. Guo, Y. Zhen, L. Yue, G. Xue, F. Fu, AgBr quantum dots decorated mesoporous Bi_2WO_6 architectures with enhanced photocatalytic activities for methylene blue, J. Mater. Chem. A. 2 (2014) 11716–11727, https://doi.org/10.1039/C4TA01444H.

[86] C. Lu, Y. Wu, F. Mai, W. Chung, C. Wu, W. Lin, C. Chen, Degradation efficiencies and mechanisms of the ZnO-mediated photocatalytic degradation of Basic Blue 11 under visible light irradiation, J. Mol. Catal. Chem. 310 (2009) 159–165, https://doi.org/10.1016/j.molcata.2009.06.011.